

# Orientalional correlations and the effect of spatial gradients in the equilibrium steady state of hard rods in 2D : A study using deposition-evaporation kinetics

Mahendra D. Khandkar and Mustansir Barma

*Department of Theoretical Physics, Tata Institute of Fundamental Research,  
Homi Bhabha Road, Colaba, Mumbai-400 005, INDIA.*

(Dated: July 21, 2018)

Deposition and evaporation of infinitely thin hard rods (needles) is studied in two dimensions using Monte Carlo simulations. The ratio of deposition to evaporation rates controls the equilibrium density of rods, and increasing it leads to an entropy-driven transition to a nematic phase in which both static and dynamical orientational correlation functions decay as power laws, with exponents varying continuously with deposition-evaporation rate ratio. Our results for the onset of the power-law phase agree with those for a conserved number of rods. At a coarse-grained level, the dynamics of the non-conserved angle field is described by the Edwards-Wilkinson equation. Predicted relations between the exponents of the quadrupolar and octupolar correlation functions are borne out by our numerical results. We explore the effects of spatial inhomogeneity in the deposition-evaporation ratio by simulations, entropy-based arguments and a study of the new terms introduced in the free energy. The primary effect is that needles tend to align along the local spatial gradient of the ratio. A uniform gradient thus induces a uniformly aligned state, as does a gradient which varies randomly in magnitude and sign, but acts only in one direction. Random variations of deposition-evaporation rates in both directions induce frustration, resulting in a state with glassy characteristics.

PACS numbers: 64.60.Cn

## I. INTRODUCTION

An assembly of particles interacting via hard-core repulsion serves as a useful model for studying simple fluids, colloids, liquid crystals and many other soft matter systems. The analysis of such model systems helps in understanding the features of real systems, such as their phase behaviour, structural and dynamic properties. An important role is played by the anisotropy of shape of the constituent particles, which can range from thick elongated platelets to thin rods. Some examples of systems in which the constituent particles show anisotropy are certain types of colloids, liquid crystals and protein molecules. In particular, rod-like particles are found in suspensions of the tobacco mosaic virus [1], nematic liquid crystals [2] and, recently, carbon nanotube gels [3]. All these systems show very rich and characteristic phase behaviour.

Rod-like particles have been modeled theoretically as ellipses [4], rectangles and spherocylinders [5, 6, 7] with varying aspect ratios, a limiting case being infinitely thin hard rods or needles [8]. These systems exhibit a number of interesting entropy-driven phase transitions which have been studied in two and three dimensions, usually using simulations with number-conserving dynamics. On the other hand, there are a number of physical processes which involve adsorption (deposition) and desorption (evaporation) of particles, which do not conserve particle number and which are important for some monolayer growth processes. Adsorption and desorption are also important in the binding/unbinding of ligands to microtubules, the interaction of proteins with DNA [9, 10] and many catalytic reactions. Finally, in recent experiments on assemblies of long objects (rice grains, thin

metal rods) on a vibrating plate [11], individual particles jump off and return to the plate, leading ultimately to a state with interesting patterns. These considerations motivate us to study the deposition and evaporation of hard objects with rigid boundaries on a substrate. While a deposition-only system, of the type studied in random sequential adsorption [9], can end up in a non-evolving jammed configuration, with the addition of evaporation, the system eventually reaches an equilibrium steady state with a density governed by the rates of deposition and evaporation [12-17]. While most of these studies have focussed on the kinetics of approach to steady state, in this paper, we are interested in the properties of the steady state itself. Specifically, we study the patterns formed due to deposition and evaporation of infinitely thin hard rods (needles) on a 2D substrate. Needles are a limiting case of rod like particles in the systems mentioned earlier. Though not directly applicable to any physical system, this is an important limiting case; the limit of zero width simplifies the problem by eliminating the aspect ratio as a parameter. The hard core constraint is enforced by rejecting any deposition event which results in an overlap of needles.

It is useful to recall some known facts about a system of hard needles with no externally imposed spatial inhomogeneities. This system shows a transition from a low-density orientationally disordered (isotropic) state to a high-density ordered state with nematic correlations. This transition, whose existence was pointed out by Onsager [18], can be viewed as an outcome of the interplay between orientational and translational entropy of the needles; the ordered (aligned) state is preferred at high density since alignment leads to an increase of translational entropy, albeit at the cost of orientational entropy. The nature of the orientational ordering is dimension-

dependent. In three dimensions, orientational long range order (LRO) sets in. A state with LRO would break the continuous symmetry of rotations, and is thus not expected to occur in 2D, even though the Mermin-Wagner theorem cannot be generalized to this system [19]. Indeed, the simulation study of Frenkel and Eppenga [8] on a system with a fixed number of needles confirms the absence of LRO in 2D, and finds a phase with power-law decays of orientational correlations, quite analogously to the XY model [20].

On a coarse-grained scale, the local orientation at location  $\mathbf{r}$  and time  $t$  is specified by an angle field  $\theta(\mathbf{r}, t)$ . The orientational correlation functions of interest are defined as

$$g_\ell(\mathbf{r}, t) = \langle \cos[\ell(\theta(\mathbf{r}, t) - \theta(0, 0))] \rangle \quad (1)$$

where  $\ell$  is an even integer, and  $\theta$  and  $\theta + \pi$  represent the same state. Quadrupolar correlations are probed by  $\ell = 2$ , whereas higher values of  $\ell$  correspond to higher multipolarities. From numerical simulations, we find power law decays in both space and time:  $g_\ell(r, 0) \sim r^{-\eta_\ell}$  and  $g_\ell(0, t) \sim t^{-\beta_\ell}$  for both  $\ell = 2$  and 4. Our results for the static correlations conform to the Kosterlitz-Thouless theory for the onset of correlations, while our results for the dynamics show that their decay in time is governed by the Edwards-Wilkinson equation. We also study spatial variations of the deposition rate, and find strong effects on the nature of the ordering. We consider several types of variations: (i) a sharp change across a linear interface; (ii) a smooth linear gradient; (iii) a random variation of rates in one direction and (iv) random variation of rates in the plane. We find that the qualitative effect of spatial variations is to induce alignment of needles in the direction of gradient, an effect with an entropic origin. In (i), the effect dies down slowly with increasing distance from the interface, but in cases (ii) and (iii) it results in a state with overall alignment along the direction of variation of the deposition rate. The random variation in (iv) induces frustration and the result is then a state with glassy features such as strong initial condition dependence and slow relaxation.

## II. MODEL AND PROCEDURE

In our model, infinitely thin hard rods (needles) are added to a 2D substrate with area  $A$  with a constant attempt rate, and simultaneously removed randomly from the substrate with a specified rate. In a deposition attempt, the location of the centre of mass of the needle is chosen at random on the substrate, and the orientation angle is chosen at random as well. Let  $\Gamma_d$  be the rate of attempted depositions per unit area per unit angle interval. An attempt is successful only if the depositing needle in question would not overlap with existing needles on the substrate; otherwise it is rejected.

During evaporation, a needle is chosen at random from those present on the substrate and then removed. If the

total rate of such removals is  $R_e$  we may associate a removal rate  $\Gamma_e = \frac{R_e}{2\pi A}$  per unit area per unit angle interval. The ratio

$$\kappa = \frac{\Gamma_d}{\Gamma_e} \quad (2)$$

of deposition to evaporation rates is the control parameter in the problem. As we show below,  $\kappa$  is related to the fugacity  $z = e^{\beta\mu}$  of an equilibrium grand canonical system.

The model under consideration can be thought of as describing the adsorption and release of needle-like gas molecules on a substrate in contact with a gas reservoir with which it can exchange particles. The equilibrium state on the substrate is then described by the grand canonical ( $\mu AT$ ) ensemble, where  $\mu$ ,  $A$  and  $T$  are respectively the chemical potential, substrate area and temperature. Define scaled coordinates  $\mathbf{s}_i = \mathbf{r}_i/L$ , where  $\mathbf{r}_i$  is the position of the  $i^{\text{th}}$  particle on the substrate and  $L$  is the linear dimension of the system. The grand canonical partition function can be written [21] as

$$\mathcal{Z} = \sum_{N=0}^{\infty} \frac{z^N}{N!} (A/\Lambda^2)^N \int d\mathbf{s}_1 \int d\mathbf{s}_2 \dots \int d\mathbf{s}_N \int d\theta_1 \int d\theta_2 \dots \int d\theta_N e^{-\beta U(\mathbf{s}_1, \mathbf{s}_2, \dots, \mathbf{s}_N, \theta_1, \theta_2, \dots, \theta_N)} \quad (3)$$

where  $\Lambda = (\frac{2\pi\hbar^2}{mk_B T})^{1/2}$  is the thermal wavelength which results from integrating over the momentum of needles, and  $U$  is the interaction energy for a configuration in which there are  $N$  needles with scaled centre of mass locations  $(\mathbf{s}_1, \mathbf{s}_2, \dots, \mathbf{s}_N)$  and orientations  $(\theta_1, \theta_2, \dots, \theta_N)$ . The corresponding equilibrium probability density of a configuration  $C \equiv (\mathbf{s}_1, \mathbf{s}_2, \dots, \mathbf{s}_N, \theta_1, \theta_2, \dots, \theta_N)$  is [21]

$$P_{eq}(C) = \frac{1}{\mathcal{Z}} \frac{z^N}{N!} (A/\Lambda^2)^N e^{-\beta U(\mathbf{s}_1, \mathbf{s}_2, \dots, \mathbf{s}_N, \theta_1, \theta_2, \dots, \theta_N)} \quad (4)$$

For our system of hard core needles, the interaction energy  $U \rightarrow \infty$  when needles overlap, while  $U = 0$  when there is no overlap between any needles. Thus all allowed configurations with fixed  $N$  have equal weights.

Deposition - evaporation dynamics involves changes of  $N$ . The evolution from a configuration  $C$  to a configuration  $C'$  can be described by the master equation

$$\frac{\partial P(C)}{\partial t} = \sum_{C'} [P(C')W(C' \rightarrow C) - P(C)W(C \rightarrow C')] \quad (5)$$

The steady state of Eq. (5), obtained by setting  $\frac{\partial P(C)}{\partial t} = 0$ , is in fact an equilibrium state if the condition of detailed balance

$$\frac{W(C' \rightarrow C)}{W(C \rightarrow C')} = \frac{P_{eq}(C)}{P_{eq}(C')} \quad (6)$$

is satisfied for every pair of configurations  $C$  and  $C'$  that can be reached from each other. Now, let  $C$  denote an  $N$ -needle configuration and let  $C'$  be the  $(N-1)$ -needle configuration obtained from  $C$  by removing a particular needle. Using Eq.(4) in Eq.(6), we see that  $\frac{\Gamma_d}{\Gamma_e} = \frac{zA}{\Lambda^2 N}$ . Thus, the steady state of deposition-evaporation dynamics is described by the grand canonical equilibrium state with

$$\kappa = \frac{z}{\rho\Lambda^2} \quad (7)$$

where  $\rho = \frac{N}{A}$  is the areal density of needles.

In our Monte Carlo studies we varied the control parameter  $\kappa$  in the range 1 to 40 and monitored the resulting density and orientational correlations. We used an  $L \times L$  substrate (with  $L = 15$  and  $25$ ) where  $L$  is in units of needle length. For each value of  $\kappa$  we made multiple runs, allowing up to  $10^7$  Monte Carlo time steps for equilibration. The Monte Carlo time  $t$  is defined as the number of attempts divided by  $L^2$ . Averaging was done over 10 sets of independent runs and 1000 configurations from each run after equilibration.

Figure 1(a) shows the variations of the density with  $\kappa$ , while Fig. 1(b) shows  $\rho$  plotted against  $z/\Lambda^2 = \rho\kappa$ . The inset in Fig. 1(a) shows a marked change in the dependence of  $\rho/(\kappa-1)$  on  $\kappa$  for  $\kappa$  in the range 20-25. As we shall see, there is a transition to a phase with power law decay of orientational correlations beyond  $\kappa = \kappa_c \simeq 25$ , as illustrated by the representative configurations shown in Fig. 2 for different values of  $\kappa$ . We turn to a quantitative study of orientational ordering in the next section.

### III. ORIENTATIONAL ORDERING

#### A. Order parameter

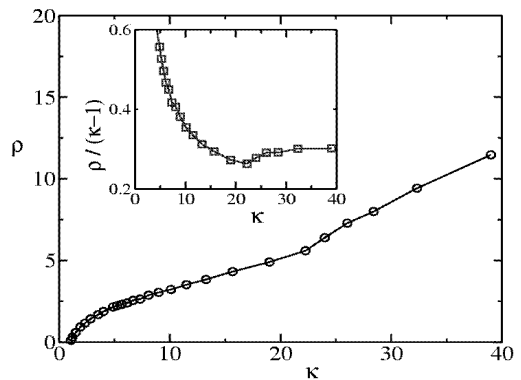
For a system of  $N$  hard rods in 2D, the nematic order parameter  $q$  is given by

$$q = \frac{1}{N} \left\langle \sum_{i=1}^N \cos(2\theta_i) \right\rangle \quad (8)$$

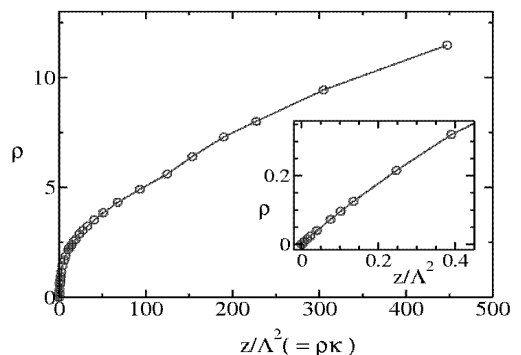
where  $\theta_i$  is the angle made by the  $i^{\text{th}}$  rod with the nematic director, which itself has an orientation  $\phi$  with respect to a fixed reference X-axis. Both  $\phi$  and  $q$  can be found by studying the tensor order parameter defined as

$$\mathbf{Q}_{\alpha\beta} = \frac{1}{N} \left\langle \sum_{i=1}^N [2u_\alpha(i)u_\beta(i) - \delta_{\alpha\beta}] \right\rangle \quad (9)$$

where  $u_\alpha(i)$  is the  $\alpha^{\text{th}}$  component of  $\mathbf{u}(i)$ , the vector specifying the orientation of the  $i^{\text{th}}$  rod. The eigenvalues of  $\mathbf{Q}_{\alpha\beta}$  are  $\pm q$ , and the corresponding eigenvectors pick out directions along and perpendicular to the director orientation  $\phi$ . Insofar as there is no long range order in the 2D



(a)



(b)

FIG. 1: (a) The variation of  $\rho$  (number of rods per unit area) with  $\kappa$  shows a change of behaviour for  $\kappa$  in the range 20-25. This is more prominently depicted in the inset which shows the variation of  $\rho/(\kappa-1)$ . (b) Variation of  $\rho$  with  $z/\Lambda^2$ . The inset shows the initial portion of the curve.

needle system,  $q$  vanishes in the thermodynamic limit. In simulations on finite systems, though,  $q$  may appear to be non-zero (Fig. 2(d)), over short times. Tracking the onset of such an apparent value is not a reliable way to locate the transition point.

#### B. Orientational cumulant of $q$

A better indication of the transition point, and also the nature of the ordered phase, is provided by monitoring the probability distribution functions  $P_L(q)$  of  $q$ , where  $q$  is the block-averaged value of the local order parameter with the system divided into blocks of finite size  $L$  [22]. A measure of the non-Gaussian character of  $P_L(q)$  is provided by the reduced 4<sup>th</sup> order Binder cumulant of  $q$

$$U_L = 1 - \frac{\langle q^4 \rangle_L}{3\langle q^2 \rangle_L^2} \quad (10)$$

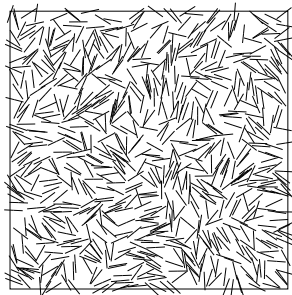
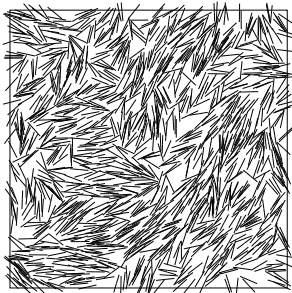
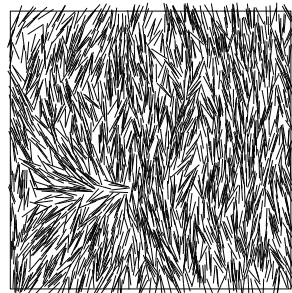
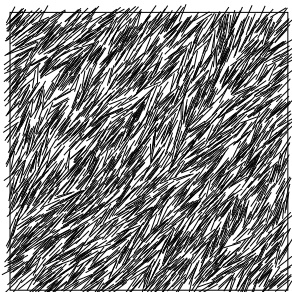
(a)  $\kappa \simeq 19$ (b)  $\kappa \simeq 24$ (c)  $\kappa \simeq 32$ (d)  $\kappa \simeq 39$ 

FIG. 2: Snapshots of hard rod configurations at different values of  $\kappa$ . The substrate size is  $15 \times 15$ . Observe the formation of defects in the configurations (a), (b) and (c).

where  $L$  is the linear size of the sub-system (block).  $U_L$  provides a useful diagnostic tool to monitor the ordering induced by varying  $\kappa$  [24].

For  $L \ll \xi$ ,  $U_L$  is expected to stay close to a fixed point value  $U^*$ . Thus, the occurrence of a critical point with  $\xi = \infty$  can be identified by plotting  $U_L$  against  $\kappa$  for various values of  $L$ , and looking for common intersection point.

We analysed the Monte Carlo data of our model by monitoring  $U_L$  (Eq. 10). The analysis was performed as follows : We simulated a single large system of size  $K \times K$  ( $K = 25$ ) and divided it into subsystems of size  $L \times L$ , thereby having total  $M^2$  number of subsystems with  $M = K/L$  [23]. Then,  $M$  was incremented in integer steps starting from 1 and  $U_L$  was estimated for those subsystem sizes  $L$  where a good analysis is possible. Consequently, we did not consider very small or very large values of  $M$ . Also, the curve for  $M = 12$  lies anomalously low and was not included. The number of subsystems ( $M$ ) we use for estimating the cumulant range from 8 to 20. Fig. 3 shows the variation of  $U_L$  as a function of  $\kappa$  for various values of  $L$ .

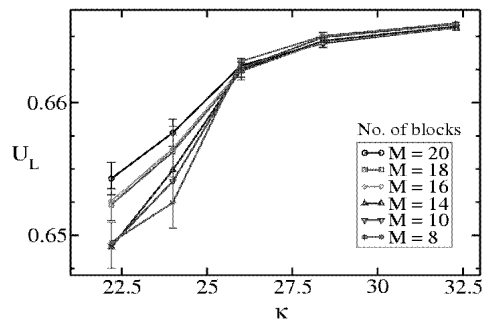


FIG. 3: Orientational cumulants  $U_L$  as a function of deposition-evaporation ratio  $\kappa$  for various subsystem sizes  $L = K/M$ . Note the collapse of the curves beyond  $\kappa_c \simeq 25$ , pointing to the occurrence of a power law phase.

Below  $\kappa_c \simeq 25.8$ , the curves are separate and distinct, but they collapse at  $\kappa_c$ , indicating the onset of ordering (Fig. 3). Moreover, the curves seem to stay collapsed for  $\kappa > \kappa_c$  suggesting that  $\xi$  remains infinite in this phase, i.e. this is a phase with power law decay of correlations. Corroboration of this is provided by directly monitoring the correlation functions as described below.

### C. Orientational correlation functions

Let us define a general orientational correlation function  $g_\ell(\mathbf{r}, t) = \langle \cos[\ell(\theta(\mathbf{r}, t) - \theta(0, 0))] \rangle$  where  $\ell$  is an even integer. We studied static and dynamical properties by investigating  $g_\ell(r, 0)$  and  $g_\ell(0, t)$ . We calculated spatial correlations by forming circular bins around each rod in turn, computing  $g_\ell(r, 0)$  for each bin, repeating this pro-

cess for all rods in the configuration and averaging over all rods (see Fig. 4). The dynamical correlation function,  $g_\ell(0, t)$  was calculated by coarse-graining. The system was divided into a number of small cells ( $1 \times 1$ ) and an average value of orientation was assigned to each cell by averaging over the orientations of those needles whose centres of mass lie in the cell. The value of  $g_\ell(0, t)$  was computed using this average value over each time frame, and averaging over all the cells (see Fig. 5). The initial drops of the curves in Figs. 4(b) and 5(b) are sensitive to the size of the cell used, while the power laws seen at the larger times do not depend on the cell size.

In the nematic-like phase, i.e. for  $\kappa$  beyond  $\kappa_c$ , the correlations decay algebraically  $g_\ell(r, 0) \sim r^{-\eta_\ell}$  and  $g_\ell(0, t) \sim t^{-\beta_\ell}$ . There are pronounced finite size effects which lead to a flattening of the curves for  $r \approx L/2$ , limiting the range over which the power law behaviour extends. We found that the values of the exponents  $\eta_\ell$  and  $\beta_\ell$  vary continuously with  $\kappa$  as shown in Table I. The estimations were done over 10 independent sets of configurations, each averaged over 1000 configurations. For  $\kappa \simeq \kappa_c$ , we observed that  $\eta_2 \simeq 0.23 \pm 0.03$  close to the predicted Kosterlitz-Thouless value 0.25. Our results for the static case, agree with those reported by Frenkel and Eppenga [8] for the case of a fixed number of hard rods on 2D plane. We confirm that at the critical point  $\kappa = \kappa_c$ , the mean density is  $\simeq 7$  [8].

For  $\kappa > \kappa_c$ , it was observed that exponents obtained from static correlations  $g_2(r)$  and  $g_4(r)$  are related through  $\eta_2 \simeq \eta_4/4$ . It was also found that the exponents derived from the temporal correlations  $g_2(t)$  and  $g_4(t)$  are related in a similar way, i.e.  $\beta_2 \simeq \beta_4/4$ . Further, the ratios  $\eta_\ell/\beta_\ell \simeq 2.0$  for  $\ell = 2$  and 4, implying that the dynamical exponent  $z_{dyn}$  is 2. These observations can be understood on the basis of the simple model discussed below.

In order to model the dynamics we note that the stochastic evaporation and deposition events change the local value of the coarse-grained angle field  $\theta$  in a noisy, diffusive way. In the discussion below, we take the angle to be an unconstrained variable running from  $-\infty$  to  $+\infty$  with  $(\theta + n\pi)$  denoting the same needle orientation for integer  $n$ . We consider a simple phenomenological equation

$$\frac{\partial \theta}{\partial t} = K \nabla^2 \theta + \xi \quad (11)$$

where  $\xi$  denotes white noise which satisfies

$$\langle \xi(\mathbf{r}, t) \xi(\mathbf{r}', t') \rangle = B \delta(\mathbf{r} - \mathbf{r}') \delta(t - t') \quad (12)$$

where  $B$  is a constant. This is of the same form as the Edwards-Wilkinson equation [25], which describes the evolution of a fluctuating interface. In our context, Eq.(11) follows from the symmetric form of the Frank free energy  $F = \frac{1}{2} K \int (\nabla \theta)^2 d\theta$  on using the phenomenological Langevin equation  $\frac{\partial \theta}{\partial t} = \frac{-\delta F}{\delta \theta} + \xi$ . A more complete description would involve coupled equations for the non-conserved density and orientational fields. From Eq.(11)

and (12) it follows that

$$\langle \theta(\mathbf{r} + \mathbf{r}', t + t') \theta(\mathbf{r}, t) \rangle = \frac{B}{64\pi^5 K} \int \frac{d^2 k}{k^2} e^{i\mathbf{k} \cdot \mathbf{r}'} e^{-K k^2 t'} \quad (13)$$

Setting  $t' = 0$  we find that

$$\langle [\theta(\mathbf{r} + \mathbf{r}', t) - \theta(\mathbf{r}, t)]^2 \rangle = \frac{B}{32\pi^5 K} \times 2\pi \ln(r) \quad (14)$$

which, using the Gaussian property of  $\theta$ , further implies

$$\langle \cos\{\ell(\theta(\mathbf{r} + \mathbf{r}', t) - \theta(\mathbf{r}, t))\} \rangle \simeq r^{-\eta_\ell} \quad (15)$$

where  $\eta_\ell = \ell^2 B / 32\pi^4 K$ . The measured values of  $\eta_\ell$  can be used to find  $K/B$ , whose value is included in Table I.

Similarly, setting  $r' = 0$  in Eq.(13) we find the autocorrelation function

$$\langle \cos\{\ell(\theta(\mathbf{r}, t + t') - \theta(\mathbf{r}, t))\} \rangle \simeq t^{-\beta_\ell} \quad (16)$$

where  $\beta_\ell = \ell^2 B / 64\pi^4 K$ . Thus, for all  $\kappa > \kappa_c$  the ratio of  $\eta_4$  to  $\eta_2$  (and  $\beta_4$  to  $\beta_2$ ) is expected to be 4; as we have seen above, our numerical results confirm this. Also, we find the dynamical exponent  $z_{dyn} = \eta_\ell / \beta_\ell$  is  $\simeq 2.0$ .

#### IV. EFFECT OF INHOMOGENEOUS $\kappa$

In this section, we explore the effects of having a spatial variation of the deposition-evaporation rate ratio  $\kappa$ . In a physical system, such a variation could arise from the variation of the chemical potential or substrate temperature from one spot to another as their local values could influence the local detachment rate, as seen from Eq. (7). As expected, such changes in  $\kappa$  induce a spatial variation of the density; more interestingly, they have a strong effect on the orientational order as well. We explore these effects by considering several types of spatial variations of  $\kappa$ .

In parallel to the discussion in section II, let  $\Gamma_d(x)$  and  $\Gamma_e(x)$  denote the deposition and evaporation rates at point  $x$  in the plane, and let  $\kappa(x) = \frac{\Gamma_d(x)}{\Gamma_e(x)}$ . Let  $C'$  be the configuration reached from configuration  $C$  by removing the rod at  $x_m$  and let  $P(C')$  and  $P(C)$  be the weights of the respective configurations in steady state. We can check that the condition of detailed balance is valid when  $P(C)$  has the product form  $P(C) = \prod_i z(x_i)$  where  $z(x_i) = \Lambda^2 \rho(x_i) \kappa(x_i)$  is the local fugacity at the location of the  $i^{th}$  rod. If  $C'$  is obtained from  $C$  by evaporating the  $m^{th}$  rod, then evidently  $P(C) = P(C') \times z(x_m)$ . Recalling that  $W(C' \rightarrow C) = \Gamma_d(x_m)$  and  $W(C \rightarrow C') = \Gamma_e(x_m)$ , we see that the condition of detailed balance is valid.

Thus the system reaches an equilibrium steady state which, however, is inhomogeneous in density, due to the non-uniform position dependence of  $\kappa$ . The nature of orientational order depends strongly on the way in which  $\kappa$  is specified to vary over the plane. Below we consider several types of variations

(i) A single interface separating low and high  $\kappa$  regions,

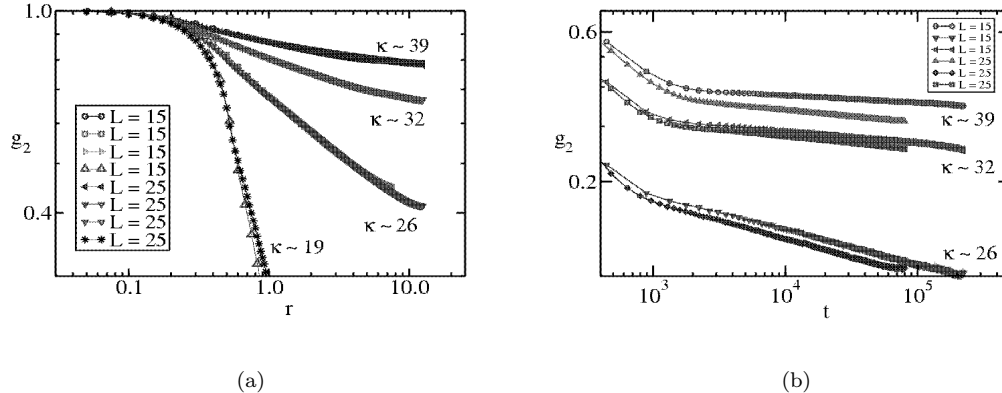


FIG. 4: Log-log plots of (a)  $g_2(r, 0) = \langle \cos[2(\theta(r, t) - \theta(0, t))] \rangle$  and (b)  $g_2(0, t) = \langle \cos[2(\theta(r, t) - \theta(r, 0))] \rangle$  showing the static and temporal behaviour respectively of  $g_2(r, t)$ . Data is shown for systems of sizes  $15 \times 15$  and  $25 \times 25$ , and different values of  $\kappa$ . The distance  $r$  is in units of rod length and time  $t$  is in Monte Carlo time steps.

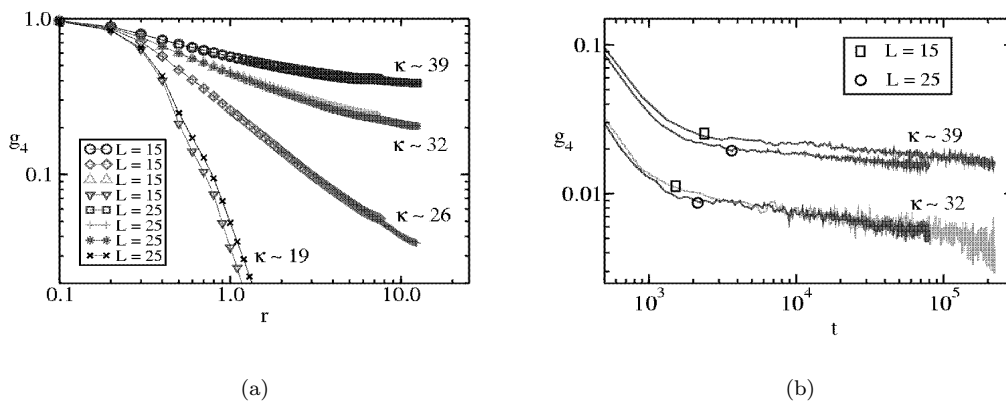


FIG. 5: Log-log plots of (a)  $g_4(r, 0) = \langle \cos[4(\theta(r, t) - \theta(0, t))] \rangle$  and (b)  $g_4(0, t) = \langle \cos[4(\theta(r, t) - \theta(r, 0))] \rangle$  showing the static and temporal behaviour respectively of  $g_4(r, t)$ , for the same system sizes and values of  $\kappa$  as in Fig. 4.

$$\begin{aligned} \kappa(x) &= \kappa_1, \text{ for } x < \frac{L}{2}, \\ \kappa(x) &= \kappa_2, \text{ for } x > \frac{L}{2}. \end{aligned}$$

(ii) A uniform gradient in  $\kappa$  across the substrate,

$$\kappa(x) = \kappa_1 \left( 1 + \alpha \frac{x}{L} \right)$$

(iii) Random variation of  $\kappa$  in the X-direction only,

$$\kappa(x) = \kappa_1 + \delta\kappa(x)$$

where  $\delta\kappa(x) < \kappa_1$  is a random function of  $x$ .

(iv) A random binary assignment of  $\kappa$  on a grid on the 2D substrate

In the first three cases, periodic boundary conditions were applied in Y-direction and open boundary conditions along X. In the last case, open boundaries were used in both directions. In all the cases considered, the

ranges of  $\kappa$  values were chosen to be above  $\kappa_c$ , the critical value in the uniform case. Our findings are as follows :

#### A. $\kappa_1 - \kappa_2$ interface

Here, a uniform value  $\kappa_1$  operates upto half-way across the 2D plane along the X-direction, while  $\kappa = \kappa_2 (> \kappa_1)$  in the remaining half. In the vicinity of the interfacial region, the rods are observed to orient in the direction of the  $\kappa$  gradient i.e. perpendicular to the interface (see Fig. 6(a)).

This can be understood on entropic grounds. That arrangement of rods is favoured which maximizes the entropy. By symmetry, the preferred average orientation of rods should be either (a) parallel or (b) perpendicular to the interface. Consider those rods in the high- $\kappa$

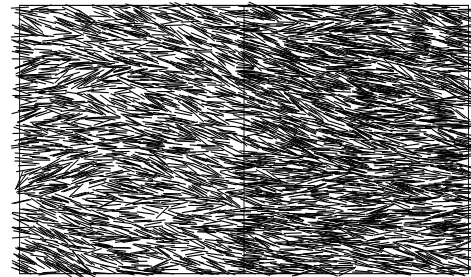
TABLE I:  $\kappa$  dependence of exponents  $\eta_\ell$  and  $\beta_\ell$  for  $\ell = 2$  and  $4$ . The estimated error is indicated in the brackets.

$\kappa$	$\rho$	$\eta_2$	$\eta_4$	$\beta_2$	$\beta_4$	$K/B$
26.0	7.3	0.23 (0.03)	0.87 (0.06)	0.11 (0.04)	0.31 (0.06)	$5.3 \times 10^{-3}$
32.3	9.4	0.098 (0.006)	0.41 (0.02)	0.037 (0.007)	0.16 (0.04)	$12.8 \times 10^{-3}$
39.0	11.4	0.059 (0.003)	0.25 (0.01)	0.022 (0.003)	0.09 (0.01)	$21.4 \times 10^{-3}$

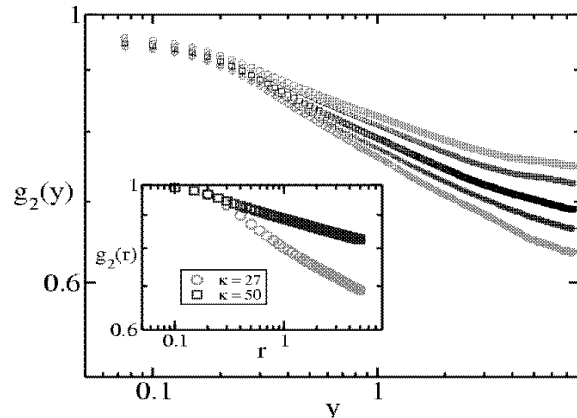
half, whose centres lie very close to the interface (within half a rod length) so that part of such rods can reach into the low density side. Small variations in the angle of each rod would contribute to the entropy, but these are limited by the presence of other rods. A horizontal average alignment allows the rods to sample a less dense environment, and thus be subject to fewer constraints, on one side. Thus, option (b) would be preferred over (a). The effect of interface-induced horizontal alignment is felt for some distance away from the interface on both sides. This is evident in Fig.6(a), which shows a steady state configuration in a system of size  $25 \times 15$  (in units of rod length), with  $\kappa_1 = 30$  and  $\kappa_2 = 50$ . However, for a large enough size, the system reverts to a power-law phase in the region far from the interface as observed in the uniform  $\kappa$  case. The correlation function decays as a power law in the bulk, away from the interface, as shown in Fig.6(b).

We also considered the case with two values of  $\kappa$ , using periodic boundary conditions in both directions which leads to two interfaces (Fig. 7). The figure shows a  $80 \times 15$ -sized system with periodically linked left and right quarters with  $\kappa_1 = 30$ , while the middle half has  $\kappa_2 = 50$ . Evidently, this system too shows interface-induced horizontal alignment. This geometry admits of an interesting limit where the entropy driven alignment is particularly clear. On shrinking the width of the central region to zero, at the same time taking the limit  $\kappa_1 \rightarrow 0$ , we obtain a 1D model as a limiting case. In this model, deposition and evaporation moves are allowed with needle centres constrained to lie on the line. Needles are found to orient preferentially perpendicular to the line (see the inset in Fig. 8). The reason is evident. If the mean orientation of the director is perpendicular to the substrate, needles have the largest leeway to make angular excursions about the mean - i.e. the rotational entropy is then the largest. The variation with  $\kappa$  of the density and order parameter  $q = \langle \cos 2\phi \rangle$  where  $\phi$  is the angle made with the direction perpendicular to the line, is shown in Fig. 8.

A similar effect should also lead to rods getting aligned horizontally if they are close to an open boundary in the 2D system. That this is so can be seen in Fig. 9, which shows a system with uniform  $\kappa = 27$  and open boundary conditions along the X-direction.



(a)



(b)

FIG. 6: (a) Snapshot of a typical hard rod configuration with a single  $\kappa_1 - \kappa_2$  interface. The system size is  $25 \times 15$  and  $\kappa_1 = 30$  (left half) and  $\kappa_2 = 50$  (right half). Boundary conditions : Open (along X) , Periodic (along Y). Notice the difference in density in the two halves. (b) This plot shows the decay of the orientational correlation function  $g_2(\mathbf{y}) = \langle \cos[2(\theta(\mathbf{y}) - \theta(0))] \rangle$  calculated for a pair of points in the same vertical strip of unit width. Curves from bottom to top correspond to different strips in two halves in the configuration (a). The inset shows  $g_2(\mathbf{r}) = \langle \cos[2(\theta(\mathbf{r}) - \theta(0))] \rangle$  measured radially for a box of size  $6 \times 6$  which is positioned at the centre of each of the left and right halves of the same configuration. The distances  $r$  and  $y$  are in units of rod length.

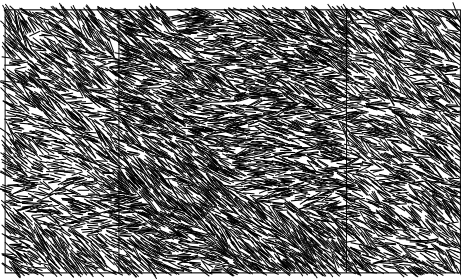


FIG. 7: A dual-interface configuration in an  $80 \times 15$ -sized system with periodic boundary conditions in both directions. The middle half of size  $40 \times 15$  and with  $\kappa_2 = 50$  separates two quarters, linked at the boundary, each of size  $20 \times 15$  and having  $\kappa_1 = 30$ .

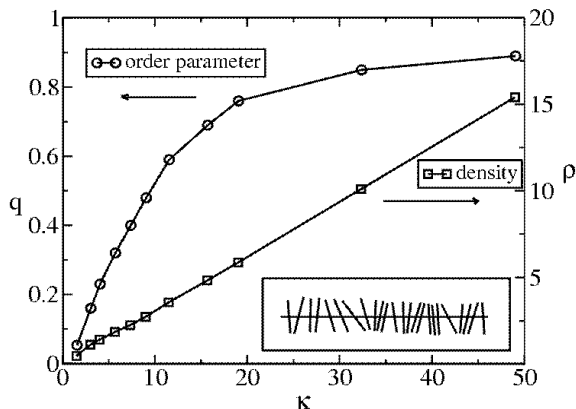


FIG. 8: Variation of the density( $\rho$ ) and order parameter( $q$ ) with  $\kappa$  for the 1D model which is a limiting case of the 2-D  $\kappa_1 - \kappa_2$  model for Fig. 7. As shown schematically in the inset, the preferred orientation of needles is perpendicular to the line.

### B. Uniform $\kappa$ gradient

This case is related to the discussion above, as the linear increase in  $\kappa$  may be viewed as a continuous succession of interfaces from one end to the other. Since each interface induces an alignment of rods across it, this results in overall alignment of the rods in the system (see Fig. 10). Note that the alignment is not an outcome of spontaneous breaking of orientational symmetry, as the gradient in  $\kappa$  singles out a direction in space. We checked that the horizontal alignment is not tied to the aspect ratio of the container by simulating a system size  $10 \times 40$ , and observing overall horizontal alignment of rods in the steady state.

Figure 10 shows a steady state configuration in a system of size  $25 \times 15$ , with  $\kappa$  varying linearly from a value  $\kappa_L = 32$  at the left end to a value  $\kappa_R = 50$  at the right end. In our simulations, the system was equilibrated for  $10^7$  MCS and  $10^4$  post-equilibration configurations were used to calculate averages. We studied

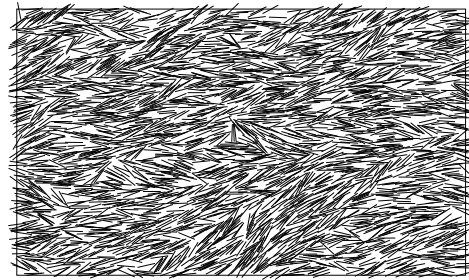


FIG. 9: A typical configuration of size  $25 \times 15$  with uniform  $\kappa = 27$  and open boundary conditions along the X-direction. Free boundaries induce alignment which propagates some distance into the bulk.

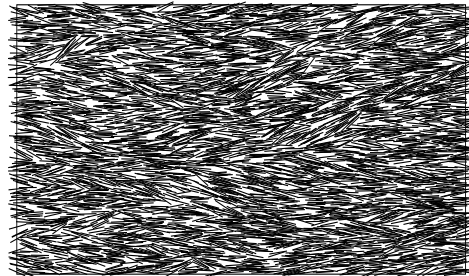


FIG. 10: A typical configuration for a  $25 \times 15$ -sized system with a uniform  $\kappa$  gradient, with  $\kappa_L = 32$  and  $\kappa_R = 50$  at the two ends respectively. The horizontal alignment induced by the gradient is evident.

the spatial and dynamical behaviour of the orientational correlation function  $g_2(r, t) = \langle \cos[2(\theta(r, t) - \theta(0, 0))] \rangle$ . Since the system is inhomogeneous along the X-direction, the substrate was divided into vertical strips, each having width of a rod length, and each strip was studied separately. The Y-density of needles inside each strip was uniform though the density varies from strip to strip. We monitored the correlation function  $g_2(y) = \langle \cos[2(\theta(y + y_0) - \theta(y_0))] \rangle$  (see Fig. 11), and found that  $g_2(y)$  decays exponentially to a non-vanishing constant value  $q_0$  which differs from strip to strip. For the system under study,  $q_0^2$  varies in the range 0.68-0.77 over the strips.

The dynamical correlation function, i.e.  $g_2(t) = \langle \cos[2(\theta(t) - \theta(0))] \rangle$  was calculated by coarse-graining. The system was divided into number of small cells ( $2 \times 2$ ) and an average value of orientation was assigned to each cell by averaging over needles in it. The plot of  $g_2(t)$  is shown in Fig. for cells at different values of X. Each curve shows an exponential approach to a non-zero constant value. The behaviour of both the spatial and dynamical orientational parts of the correlation functions indicates a phase with overall orientational alignment.



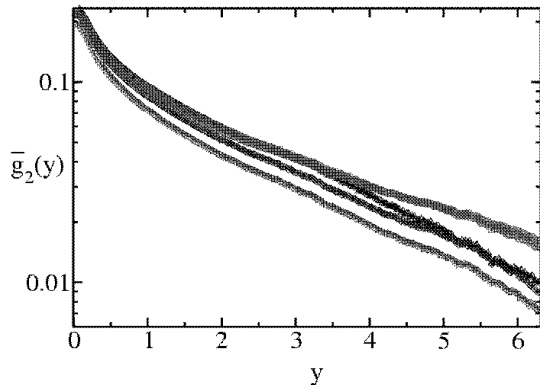


FIG. 11: Correlation function in a  $25 \times 15$ -sized system with a uniform  $\kappa$  gradient. Shown is the log-normal plot  $\bar{g}_2(y) = \langle \cos[2(\theta(y) - \theta(0))] \rangle - q_0^2$  for pairs of points in the same vertical strip of unit width. Curves from bottom to top correspond to different vertical strips in the order of increasing  $\kappa$ . It is evident from the plots that  $\bar{g}_2(y)$  exhibits exponential decay. The distance  $y$  is in units of rod length.

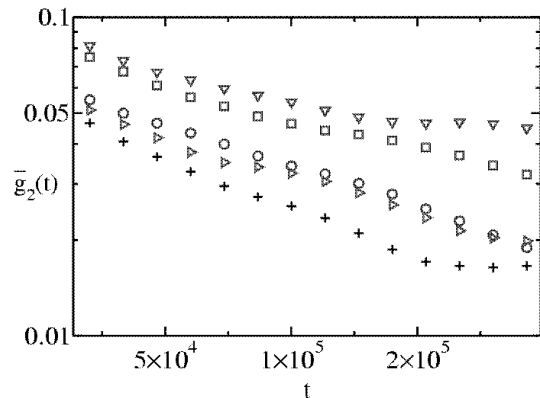


FIG. 12: Dynamical correlation function in the system of Fig. 10 and 11. Log-normal plots of  $\bar{g}_2(t) = \langle \cos[2(\theta(t) - \theta(0))] \rangle - q_0^2$  as shown, with curves from bottom to top correspond to different cells with increasing  $\kappa$  (refer to the main text for details). The time  $t$  is in Monte Carlo time steps.

### C. Random variation of $\kappa(x)$

We have seen that a uniform gradient in  $\kappa$  results in an orientationally ordered state. However, the argument for ordering does not depend on the gradient being constant in magnitude or sign. Thus, if  $\kappa$  varies randomly (with  $\kappa > \kappa_c$ ) along the X-direction but is uniform along Y, the resulting state once again should exhibit horizontal alignment with needles aligned along the X-direction. The resulting state can once again be viewed as continuous succession of interfaces and should display overall alignment.

Figure 13 shows a steady state configuration obtained with a quenched random variation of  $\kappa(x)$ . The system was simulated by varying  $\kappa$  randomly around a value of  $\kappa$  such that  $\kappa \pm \delta\kappa(x) > \kappa_c$ , where  $\delta\kappa(x)$  denotes random variations along X-direction. We used  $\kappa \simeq 32$  and  $\delta\kappa = 2.0$ . The correlation functions  $g_2(y)$  and  $g_2(t)$  behave similarly to the uniform gradient case (see Fig. 14 and 15). Thus, this case also yields a phase with overall orientational alignment.

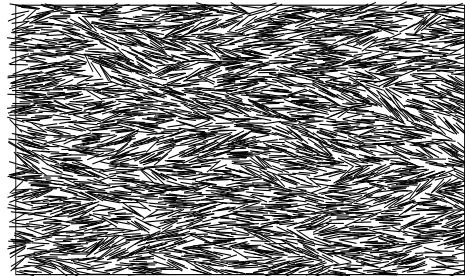


FIG. 13: A typical configuration for a  $25 \times 15$ -sized system with a  $\kappa$  gradient achieved by varying the value of  $\kappa$  randomly around 32 in the X-direction only. The horizontal alignment induced by the gradient is evident.

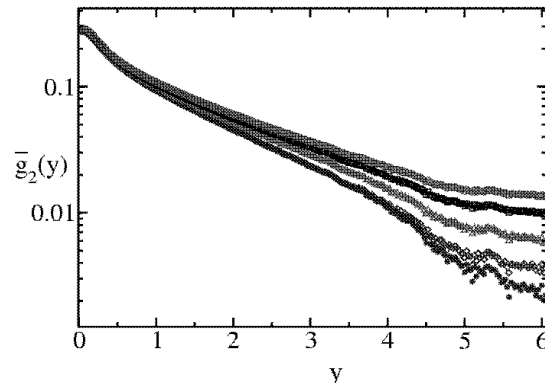


FIG. 14: Correlation function in a  $25 \times 15$ -sized system with a random  $\kappa$  gradient in the X-direction only. Shown is the log-normal plot  $\bar{g}_2(y) = \langle \cos[2(\theta(y) - \theta(0))] \rangle - q_0^2$  for pairs of points in the same vertical strip of unit width. Curves from bottom to top correspond to different vertical strips in the order of increasing  $\kappa$ . It is evident from the plots that  $\bar{g}_2(y)$  exhibits exponential decay. The distance  $y$  is in units of rod length.

### D. 2D random binary distribution of $\kappa$ values

In this case, the fugacity is set inhomogeneously in a quenched disordered fashion, so that the tendency to align locally along gradients results in competing patterns of order, i.e the system is frustrated. The resulting

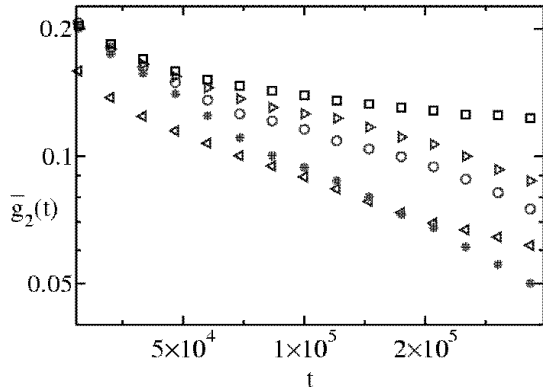


FIG. 15: Dynamical correlation function in the system of Fig. 13 and 14. Log-normal plots of  $\bar{g}_2(t) = \langle \cos[2(\theta(t) - \theta(0))] \rangle - q_0^2$  as shown, with curves from bottom to top correspond to different cells with increasing  $\kappa$ . The time  $t$  is in Monte Carlo time steps.

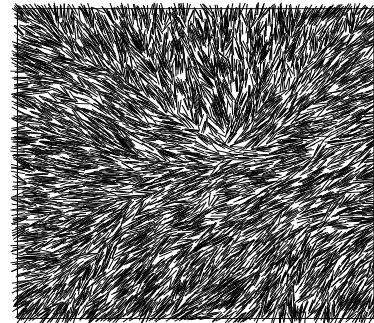
state has glassy features and contains domains of different orientations (see Fig. 16) [26].

In our simulations, we divided the substrate of size  $25 \times 25$  into a grid of unit length squares. Each square was randomly assigned a  $\kappa$  value either 27 or 50 (both greater than  $\kappa_c$ ). The random  $\kappa$  gradient across square edges generates local disorder, which can disrupt the orientational order and result in destruction of orientational alignment on the scale of the system size. The effect of quenched random disorder due to orientational randomness of cross-links in a system of nematic elastomers has been studied earlier [27] and the model was reported to have spin-glass like behaviour. In our model, the disorder emerges from the randomness in the spatial distribution of  $\kappa$  values. We find that the spatial correlation  $g_2(r)$  decays exponentially to zero (Fig. 17) whereas the dynamical part  $g_2(t)$  seems to decay in an algebraic manner to a non-zero value (Fig. 18).

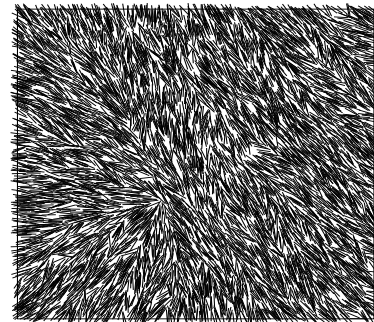
The behavior is suggestive of a glassy system which is disordered in space but relaxes slowly in time. Moreover, it was also found that with same quenched disorder arrangement, different initial conditions lead to different states. Typical configurations in each of these states are shown in Fig. 16, which is a glass-like feature.

## V. CONTINUUM DESCRIPTION

As discussed above, our simulations show that a spatially inhomogeneous deposition-evaporation ratio  $\kappa$  can induce nematic order and other interesting orientational patterns in the equilibrium state of a system of hard needles. It is interesting to ask whether these effects can be captured within a phenomenological coarse-grained description based on including symmetry-allowed terms in the free energy. In the context of liquid crystals, such an



(a)



(b)

FIG. 16: Snapshots of hard rod configurations for random binary distribution of  $\kappa$  values 27 and 50 on the substrate of size  $25 \times 25$ . Representative configurations characterizing two different states ((a) and (b)) which are reached from different initial conditions, for the same  $\kappa$  distribution.

approach has proved successful in studying large-distance phenomena, including the effects of walls and other inhomogeneities [2]. Below we sketch such a description for our system of interest [28]. Besides showing that gradients in the deposition-evaporation rates lead to orientational ordering, the treatment suggests the occurrence of local sply.

Let us define a nematic director field  $\hat{n}(r)$  to describe the local coarse-grained value of the orientation of needles (evidently,  $\hat{n}(r)$  and  $-\hat{n}(r)$  describe the same configuration). In the absence of externally imposed inhomogeneities, spatial variations of  $\hat{n}(r)$  lead to a free energy described by the Frank form [2]

$$F_K = \int d^2r \left[ \frac{K_1}{2} (\nabla \cdot \hat{n})^2 + \frac{K_3}{2} (\hat{n} \times (\nabla \times \hat{n}))^2 \right] \quad (17)$$

The two terms describe, respectively, contributions of sply and bend to the free energy; there is no contri-

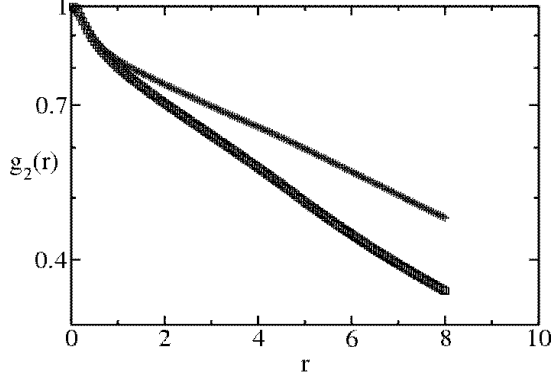


FIG. 17: Evidence for exponential decay of spatial correlations in a system with random binary distribution of  $\kappa$ . The figure shows log-normal plots of  $g_2(\mathbf{r}) = \langle \cos[2(\theta(\mathbf{r}) - \theta(0))] \rangle$ . The parameters are the same as in Fig. 16, and the curves correspond to the different steady states evolved from two different initial conditions. The distance  $r$  is in units of rod length.

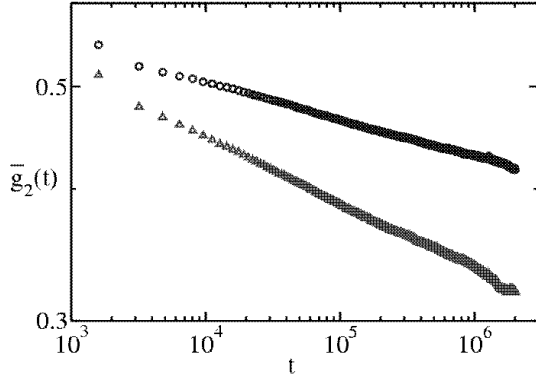


FIG. 18: Evidence for a power law decay of temporal correlations in a system with random binary distribution of  $\kappa$ . The figure shows log-log plots of  $\bar{g}_2(t) = \langle \cos[2(\theta(t) - \theta(0))] \rangle - q_0^2$ . The parameters are the same as in Fig. 16, and the curves are obtained in the different steady states reached from two different initial conditions. The time  $t$  is in Monte Carlo time steps.

bution from twist in 2-d.

Inhomogeneities in deposition-evaporation rates lead to spatial gradients  $\nabla\kappa$ , which imply new terms in the free energy. These terms consist of scalars involving  $\nabla\kappa$  and  $\hat{n}$ , respecting invariance under  $\hat{n} \leftrightarrow -\hat{n}$ . Two such scalars are obtained by replacing the gradient operator

by  $\nabla\kappa$  in the terms in Eq.(17) to get

$$F_J = \int d^2r \frac{J_1}{2} [(\nabla\kappa \cdot \hat{n})^2] + \int d^2r \frac{J_3}{2} [(\hat{n} \times (\nabla\kappa \times \hat{n}))^2] \quad (18)$$

In addition to these terms, which are quadratic in  $\nabla\kappa$ , one can also construct scalars which involve  $\nabla\kappa$  linearly [29]

$$F_L = \int d^2r \frac{L_1}{2} \nabla\kappa \cdot [\hat{n}(\nabla \cdot \hat{n})] + \int d^2r \frac{L_3}{2} \nabla\kappa \cdot [(\hat{n} \cdot \nabla)\hat{n}]. \quad (19)$$

Symmetry considerations alone do not suffice to determine the values of the coefficients  $K_1, K_3, J_1, J_3, L_1$  and  $L_3$ . Their density dependences can be found on noting that a change in  $\kappa$  induces a change in density, thereby influencing the elastic energy. To incorporate this, we replace  $\hat{n}$  in Eq. (17) by  $(\rho(r)\hat{n}/\rho_0)$  where  $\rho(r)$  and  $\rho_0$  are the local and average densities respectively. Appendix A contains the resulting form of the free energy  $F_\rho$  and the values of the coupling constants.

Let us turn to the consequences of the new terms. With a uniform spatial gradient,  $\nabla\kappa = \alpha\hat{x}$  (case (ii) above),  $F_J$  induces overall alignment of needles. To see this, consider  $F_K + F_J$ . Evidently,  $F_K$  is minimized by any arrangement in which  $\hat{n}$  is uniform in space while  $F_J$  is orientation dependent. Writing  $\hat{n} = \hat{x}\cos\phi + \hat{y}\sin\phi$ , we find

$$F_J = \alpha^2 (J_1 \cos^2\phi + J_3 \sin^2\phi) \quad (20)$$

$F_K + F_J$  is minimized by having an aligned state, either with  $\phi = 0$  (if  $J_3 > J_1$ ) or with  $\phi = \frac{\pi}{2}$  (if  $J_3 < J_1$ ). Our numerical results, supported by the entropic considerations given above, show alignment in the direction of the gradient, implying  $\Delta J \equiv J_3 - J_1$  is positive.

Now consider the effect of  $F_L$ . Setting  $\nabla\kappa = \alpha\hat{x}$  in Eq. (19), we find

$$F_L = -\alpha(L_1 + L_3) \sin\phi \cos\phi \frac{\partial\phi}{\partial x} + \alpha(L_1 \cos^2\phi - L_3 \sin^2\phi) \frac{\partial\phi}{\partial y} \quad (21)$$

$(F_K + F_L)$  can be minimized on noting that each of the  $L_1$  and  $L_3$  terms is an eigenfunction of the Frank elastic matrix. The result is

$$\frac{\partial\phi}{\partial y} = \frac{-L_1}{K_1} \cos^2\phi + \frac{L_3}{K_3} \sin^2\phi \quad (22)$$

$$\frac{\partial\phi}{\partial x} = \left( \frac{L_1}{K_1} + \frac{L_3}{K_3} \right) \cos\phi \sin\phi \quad (23)$$

These terms describe a spiralling tendency of the director in space.

The full problem involves minimizing  $F_J + F_K + F_L$ . If  $F_J$  is dominant, the director is primarily aligned along

the gradient implying  $\phi$  is small. Eqs.(22) and (23) then reduce to  $\partial\phi/\partial y \approx -L_1/K_1$  which describes a spiralling director; further,  $F_J$  restricts angular excursions to be at most  $\phi_0 \propto \frac{1}{\sqrt{\Delta J}}$ . Thus the predicted state is one with overall alignment along the gradient, but with local splay structures, each with a small opening angle  $\simeq 2\phi_0$ . This picture is borne out by our simulations.

For case (iii) in which  $\kappa(x)$  varies randomly, we see that  $F_J = \overline{\alpha^2}(J_1 \cos^2\phi + J_3 \sin^2\phi)$  where  $\overline{\alpha^2}$  is the spatial average of the mean squared gradient. As for case (ii), the free energy is minimized by having a state with alignment along the gradient, as observed in our simulations, provided  $J_3 > J_1$ .

In case (iv), the gradients that appear in Eq. (18) are random in direction leading to frustration in the arrangement of needles. Equations (17), (18) and (19) provide a starting point for a theoretical description of the glassy state that results.

## VI. CONCLUSION

In summary, we have studied orientational ordering in a 2D grand canonical system of hard rods using deposition and evaporation moves. The control parameter is the ratio  $\kappa$  of deposition and evaporation rates, which controls the density. The system with uniform  $\kappa$  displays a transition from an isotropic phase (for  $\kappa < \kappa_c$ ) to a phase characterized by algebraically decaying static and dynamical orientational correlations for  $\kappa > \kappa_c$ . Further, the values of the critical exponents and the behaviour of the orientational cumulant are consistent with Kosterlitz-Thouless theory. The numerical results for the dynamical correlation functions are described by a phenomenological Edwards-Wilkinson equation for the non-conserved orientational field.

Our principal results pertain to the new behavior induced by having a position-dependent  $\kappa$ , and hence a space-varying density of rods. An anisotropic variation of  $\kappa$  (say along the X-direction only) results in needles aligning along the  $\kappa$  gradient. This was understood by first considering the effect of an interface separating regions with two values of  $\kappa$ . Entropic considerations lead the needles to align normal to the interface, i.e. along the gradient. From another point of view,  $\kappa$ -gradients lead to new terms in the Frank-like free energy and these in turn imply orientational ordering. Finally in a system with quenched disorder corresponding to spatially random  $\kappa$ , we found indications of orientationally frozen states with glass-like characteristics. It would be useful to have a better characterization and understanding of this glassy state.

The mechanism behind gradient-induced orientational ordering is simple: spatial variations of  $\kappa$  induce variations in needle density; and an average alignment of needles along the gradient is preferred as this leads to an enhanced entropy of rotational excursions around the mean. In effect, the  $\kappa$ -gradient thus behaves like an external

field acting to produce nematic order, ultimately due to the strong coupling between spatial and orientational degrees of freedom in the needle system. Gradient-induced ordering effects should be present in three-dimensional systems as well. In 3D, the Onsager mechanism for nematic long range order would predict ordering for values of a uniform  $\kappa$  exceeding a critical value  $\kappa_c$ . The addition of a uniform  $\kappa$ -gradient would be expected to lead to a nonzero value of nematic ordering for all values of  $\kappa$ , and to enhance its value for  $\kappa > \kappa_c$ . It would be interesting to test this prediction, and have a quantitative measure of gradient-induced ordering in 3D.

## ACKNOWLEDGMENTS

We acknowledge very useful discussions with Yashodhan Hatwalne, Sriram Ramaswamy and Gautam Menon. We thank Deepak Dhar for a critical reading of the manuscript and suggestions.

## APPENDIX A

To incorporate the effect of spatial variation of the density, we write  $(\rho(r)\hat{n}/\rho_0)$  in place of the director  $\hat{n}$  in the Frank free energy  $F_K$  of Eq. (17). The resulting expression  $F_\rho$  for the free energy can be written as

$$F_\rho = \int d^2r \left[ \frac{K_1}{2\rho_0^2} (\nabla \cdot \rho\hat{n})^2 + \frac{K_3}{2\rho_0^4} (\rho\hat{n} \times (\nabla \times \rho\hat{n}))^2 \right] \quad (24)$$

The expansion of the integrand involves ten terms :

$$\begin{aligned} & \left[ \frac{K_1}{2\rho_0^2} \rho^2 \sin^2\phi + \left( \frac{K_3}{2\rho_0^4} \rho^2 \right) \rho^2 \cos^2\phi \right] (\partial\phi/\partial x)^2 \\ & + \left[ \frac{K_1}{2\rho_0^2} \rho^2 \cos^2\phi + \left( \frac{K_3}{2\rho_0^4} \rho^2 \right) \rho^2 \sin^2\phi \right] (\partial\phi/\partial y)^2 \\ & + \left[ \frac{K_1}{2\rho_0^2} \cos^2\phi + \left( \frac{K_3}{2\rho_0^4} \rho^2 \right) \sin^2\phi \right] (\partial\rho/\partial x)^2 \\ & + \left[ \frac{K_1}{2\rho_0^2} \sin^2\phi + \left( \frac{K_3}{2\rho_0^4} \rho^2 \right) \cos^2\phi \right] (\partial\rho/\partial y)^2 \\ & + \left[ \frac{-K_1}{2\rho_0^2} + \left( \frac{K_3}{2\rho_0^4} \rho^2 \right) \right] 2\rho \sin\phi \cos\phi (\partial\phi/\partial x) (\partial\rho/\partial x) \\ & + \left[ \frac{K_1}{2\rho_0^2} - \left( \frac{K_3}{2\rho_0^4} \rho^2 \right) \right] 2\rho \sin\phi \cos\phi (\partial\phi/\partial y) (\partial\rho/\partial y) \\ & + \left[ \frac{K_1}{2\rho_0^2} - \left( \frac{K_3}{2\rho_0^4} \rho^2 \right) \right] 2 \sin\phi \cos\phi (\partial\rho/\partial x) (\partial\rho/\partial y) \\ & + \left[ \frac{-K_1}{2\rho_0^2} + \left( \frac{K_3}{2\rho_0^4} \rho^2 \right) \right] 2\rho^2 \sin\phi \cos\phi (\partial\phi/\partial x) (\partial\phi/\partial y) \\ & + \left[ \frac{-K_1}{2\rho_0^2} \sin^2\phi - \left( \frac{K_3}{2\rho_0^4} \rho^2 \right) \cos^2\phi \right] 2\rho (\partial\phi/\partial x) (\partial\rho/\partial y) \\ & + \left[ \frac{K_1}{2\rho_0^2} \cos^2\phi + \left( \frac{K_3}{2\rho_0^4} \rho^2 \right) \sin^2\phi \right] 2\rho (\partial\rho/\partial x) (\partial\phi/\partial y) \end{aligned}$$

In case (ii) where  $\kappa$  varies linearly with  $x$ , the density gradient is non-zero only along the X-direction, and vanishes along Y, so the terms involving  $\partial\rho/\partial y$  do not contribute. We can then read off the density dependence induced in the elastic constants in terms of the original Frank's constants as

$$K'_1(\rho) = \frac{K_1}{\rho_0^2} \rho^2 \text{ and } K'_3(\rho) = \frac{K_3}{\rho_0^4} \rho^4$$

Now, comparing the third term of the expression with Eq. (18) and writing  $\partial\rho/\partial x = \alpha\zeta(\rho)$  where  $\zeta(\rho) = \partial\rho/\partial\kappa$ , we have

$$J_1(\rho) = \frac{K_1}{\rho_0^2} (\zeta(\rho))^2 \quad ; \quad J_3(\rho) = \frac{K_3}{\rho_0^4} \rho^2 (\zeta(\rho))^2 \quad (25)$$

Similarly, grouping the fifth and the tenth terms together and comparing with Eq. (19), we obtain

$$L_1(\rho) = \frac{K_1}{\rho_0^2} 2\rho\zeta(\rho) \quad ; \quad L_3(\rho) = \left(-\frac{K_3}{\rho_0^4} \rho^2\right) 2\rho\zeta(\rho). \quad (26)$$

- 
- [1] S. Fraden et al, Phys. Rev. Lett., **63**, 2068 (1989).  
[2] P. G. de Gennes and J. Prost, *The Physics of Liquid Crystals*, 2<sup>nd</sup> Ed. (Clarendon, Oxford, 1993).  
[3] M. F. Islam et al, Phys. Rev. Lett., **92**, 088303 (2004).  
[4] J. A. Cuesta and D. Frenkel, Phys. Rev. A, **42**, 2126 (1990).  
[5] A. Stroobants, H. N. W. Lekkerkerker and D. Frenkel, Phys. Rev. A, **36**, 2929 (1987).  
[6] M. A. Bates and D. Frenkel, J. Chem. Phys. **112**, 10034 (2000).  
[7] M. C. Lagomarsino, M. Dogterom and M. Dijkstra, J. Chem. Phys. **119**, 3535 (2003).  
[8] D. Frenkel and R. Eppenga, Phys. Rev. A, **31**, 1776 (1985).  
[9] J. W. Evans, Rev. Mod. Phys. **65**, 1281 (1993).  
[10] E. Frey and A. Vilfan, Chem. Phys. **284**, 287 (2002).  
[11] V. Narayan, N. Menon and S. Ramaswamy (unpublished).  
[12] R. B. Stinchcombe, M. D. Grynberg and M. Barma, Phys. Rev. E **47**, 4018 (1993).  
[13] P. L. Krapivsky and E. Ben-Naim, J. Chem. Phys. **100**, 6778 (1994).  
[14] A. J. Kolan, E. R. Nowak and A. V. Tkachenko, Phys. Rev. E **59**, 3094 (1999).  
[15] P. R. Van Tassel et al, J. Chem. Phys. **112**, 1483 (2000).  
[16] J. Talbot, G. Tarjus and P. Viot, Phys. Rev. E **61** 5429 (2000).  
[17] Lj. Budinski-Petkovic, U. Kozmidis-Lubiric, Physica A **301**, 174 (2001).  
[18] L. Onsager, Ann. N. Y. Acad. Sci., **51**, 627 (1949).  
[19] J. P. Straley, Physical Review A, **4**, 675 (1971).  
[20] D. R. Nelson in *Phase Transitions and Critical Phenomena* edited by C. Domb and J. L. Lebowitz (Academic London, 1983) vol. 7.  
[21] D. P. Landau and K. Binder in *A Guide to Monte Carlo Simulations in Statistical Physics* (Cambridge University Press, 2000), section 6.1.3.  
[22] K. Binder in *Monte Carlo Methods in Statistical Physics: An Introduction*, K. Binder, D.W. Heermann (Springer, Berlin, 1988).  
[23] H. Weber, D. Marx and K. Binder, Phys. Rev. B **51**, 14636 (1995).  
[24] For instance, for Ising-like systems, for  $T > T_c$  and  $L \gg \xi$ ,  $P_L(s)$  approaches a Gaussian distribution, while for  $T < T_c$  and  $L \gg \xi$ ,  $P_L(s)$  approaches two Gaussians centered at  $\pm M_0$  where  $\xi$  denotes the correlation length and  $M_0$  is the spontaneous magnetization of infinite system. At criticality,  $P_L(s)$  approaches a scaled universal form for large  $L$  [22, 23]. Note that ' $s$ ' denotes the order parameter corresponding to Ising-like systems.  
[25] S. F. Edwards and D. R. Wilkinson, Proc. Roy. Soc. Lond. A **381**, 17 (1982).  
[26] K. Binder in *Spin Glasses and Random Fields* edited by A. P. Young (World Scientific, 1997).  
[27] Y. -K. Yu, P. L. Taylor and E. M. Terentjev, Phys. Rev. Lett., **81**, 128 (1998).  
[28] We are grateful to Yashodhan Hatwalne, Gautam Menon and Sriram Ramaswamy for very useful inputs on this section.  
[29] The form of these terms is the same as those describing the coupling of a flexoelectric nematic to the electric field; see Section 3.3.2 of Ref. [2]. In our case, the external field is  $\nabla\kappa$ .